Daunorubicin induces GLI1-dependent apoptosis in colorectal cancer cell lines

BO RAM KIM[1,2*], DAE YEONG KIM[1,2*], NA LY TRAN[3*], BU GYEOM KIM[1,2], SUN IL LEE[4], SANG HEE KANG[4], BYUNG YOOK MIN[4], WOOYOUNG HUR[5,6] and SANG CHEUL OH[1,2]

[1]Division of Oncology, Department of Internal Medicine, Korea University College of Medicine, Korea University Guro Hospital, Seoul 08308, Republic of Korea; [2]Institute of Convergence New Drug Development, Korea University College of Medicine, Seoul 02841, Republic of Korea; [3]Division of Bio-Medical Science & Technology, KIST School, University of Science and Technology (UST), Seoul 02792, Republic of Korea; [4]Department of Surgery, Korea University Guro Hospital, Korea University College of Medicine, Seoul 08308, Republic of Korea; [5]Medicinal Materials Research Center, Korea Institute of Science and Technology, Seoul 02792, Republic of Korea; [6]HY-KIST Bio-convergence, Hanyang University, Seoul 04763, Republic of Korea

Received November 21, 2023; Accepted April 22, 2024

DOI: 10.3892/ijo.2024.5654

Abstract. Daunorubicin, also known as daunomycin, is a DNA-targeting anticancer drug that is used as chemotherapy, mainly for patients with leukemia. It has also been shown to have anticancer effects in monotherapy or combination therapy in solid tumors, but at present it has not been adequately studied in colorectal cancer (CRC). In the present study, from a screening using an FDA-approved drug library, it was found that daunorubicin suppresses GLI-dependent luciferase reporter activity. Daunorubicin also increased p53 levels, which contributed to both GLI1 suppression and apoptosis. The current detailed investigation showed that daunorubicin promoted the β-TrCP-mediated ubiquitination and proteasomal degradation of GLI1. Moreover, a competition experiment using BODIPY-cyclopamine, a well-known Smo inhibitor, suggested that daunorubicin does not bind to Smo in HCT116 cells. Administration of daunorubicin (2 mg/kg, ip, qod, 15 days) into HCT116 xenograft mice profoundly suppressed tumor progress and the GLI1 level in tumor tissues. Taken together, the present results revealed that daunorubicin suppresses canonical Hedgehog pathways in CRC. Ultimately, the present study discloses a new mechanism of daunorubicin's anticancer effect and might provide a rationale for expanding the clinical application of daunorubicin.

Correspondence to: Professor Sang Cheul Oh, Division of Oncology/Hematology, Department of Internal Medicine, Korea University Guro Hospital, 148 Gurodong-gil, Guro, Seoul 08308, Republic of Korea
E-mail: sachoh@korea.ac.kr

Dr Wooyoung Hur, Medicinal Materials Research Center, Korea Institute of Science and Technology, 5 Hwarangro-14-gil, Seongbuk, Seoul 02792, Republic of Korea
E-mail: whur@kist.re.kr

*Contributed equally

Key words: daunorubicin, hedgehog signaling, colorectal cancer, GLI1, p53

Introduction

The evolutionary-conserved Hedgehog (Hh) signaling pathway plays an essential role in developmental processes such as embryonic development and cell differentiation (1-5). In vertebrates, the canonical Hh pathway is triggered by the interaction between a 12-pass transmembrane protein Patched (Ptch1/2) and one of the three Hh ligands, sonic Hh (Shh), indian Hh (Ihh) and desert Hh (Dhh), of which Shh is the most potent ligand for the Hh pathway. In the absence of Hh ligands, Ptch is localized in the base of the primary cilium (PC) and suppresses the activation of GPCR-like transmembrane protein Smoothened (Smo) by indirectly blocking Smo localization to the PC, while full-length GLI is sequestered by Sufu in the cytosol and phosphorylated by PKA, GSK3β and CK1. Hyperphosphorylated GLI2/3 undergoes partial proteasomal degradation via β-TRCP-mediated ubiquitination, and the resulting truncated forms of GLI (GLI2R, GLI3R) translocate into the nucleus, where they then act as transcriptional repressors.

Upon Hh ligand binding, Ptch is internalized and degraded via Smurf-mediated ubiquitination. This causes Smo to be liberated and activated through phosphorylation by CK1 and GRK2, then translocated to the PC. At this point, Smo releases GLI transcription factors from suppressive interaction with Sufu, thus bypassing the phosphorylation and subsequent GLI2/3 cleavage. The active forms of GLI (GLI1 and GLI2A) shuffle to the nucleus and turn on the transcriptions of an array of downstream genes, including those related to the Hh pathway (for example, GLI1, Smo and Ptch1), proliferation (such as cyclinD1 and c-Myc), survival (for example, Bcl-2) and stem cell self-renewal (including Nanog and Sox2) (6).

The Hh pathway is associated with important phenotypes of cancers, such as cancer cell growth, self-renewal of cancer stem cells and anticancer drug resistance. Uncontrolled canonical Hh signaling is associated with the development of various cancer types. Almost all cases of sporadic basal cell carcinomas (BCCs) are attributable to Hh pathway activation. Loss of function mutation of Ptch1 accounts for ~90% of patients with BCC, while R562Q (Smo-M1) and W535L (Smo-M2) are the main activating Smo mutations found in the remaining BCC population (7). In the case of breast cancers, the levels of Smo and GLI1 are significantly higher in triple-negative breast cancer (TNBC) than they are in other subtypes of breast cancers, and the expression levels are correlated with tumor stages of TNBC (8). Hh ligands are highly expressed in most patients with colorectal cancer (CRC) (9), and the expression levels of Ptch1 and Smo gradually increase with the progression of CRC (10). Loss of heterozygosity or somatic mutation of Ptch1 or Sufu also occurs in numerous other cancers, including bladder cancer, esophageal squamous cell carcinoma, medulloblastoma and rhabdomyosarcoma.

Moreover, a number of studies using various cancer models have revealed that GLI transcription factors can be modulated by oncogenic signaling pathways such as Raf/MEK/ERK and PI3K/Akt signaling, independent of Hh ligand or PTCH/Smo. This so-called 'non-canonical Hh pathway' activation also plays an important role in cancer development. For example, in pancreatic ductal adenocarcinoma (PDCA), mutant K-Ras mediated Gli1 transcriptional activation is needed for cell proliferation and PDCA formation *in vivo* (11). In esophageal adenocarcinoma, mTOR-S6K1 signaling increases both the phosphorylation and transcriptional activity of GLI in a Smo-independent manner (12). In melanoma cells, the stability and activity of Gli1 is upregulated by the oncogenic WIP1 phosphatase (13).

Hence, the Hh pathway is an important cancer therapeutic target. Among the oncogenic components of Hh pathway components, Smo has represented the primary drug target, presumably because it has a large drug-binding pocket. Various classes of Smo antagonists have been developed, among which vismodegib (GDC-0449) and sonidegib (LDE225) have been FDA-approved as cancer drugs for advanced and metastatic BCC. Despite the favorable clinical efficacy of the Smo inhibitors, the patients' tumor tissues showed the emergence of drug resistance through several mechanisms, including the acquisition of drug-resistant Smo mutations, the amplification of GLI2 and its downstream genes, and the upregulation of non-canonical GLI activation signaling. This situation warrants the development of next-generation inhibitors targeting the drug-resistant mutant Smo or targeting the upregulated non-canonical GLI pathway (5).

To identify new class Hh pathway inhibitors, several groups have conducted small molecule screenings using GLI1-dependent reporter assays and identified compounds that inhibit GLI1-mediated transcription with novel modes of action. GANT-58 and GANT-61, both of which inhibit GLI1 activity in the nucleus, were identified, and GANT-61 was shown to act by interfering with GLI-DNA binding (14,15). Furthermore, a previous study involving a small molecule screening of 120,000 compounds identified four compounds (HPI-1 to 4), each with a distinct mechanism of action but relatively low potency (16). In the present study, an FDA-approved drug library was screened using GLI-luciferase reporter assay in HCT116 cells, and it was revealed that daunorubicin inhibits GLI1-dependent transcription. In the present study, it was reported for the first time, to the best of the authors' knowledge, that the anticancer activity of daunorubicin is mediated in part by the suppression of the non-canonical Hh pathway. The current study is expected to provide a rationale for expanding the clinical applicability of daunorubicin.

Materials and methods

Cell culture. The NIH3T3 cell line stably expressing GLI-luciferase reporter construct was purchased from BPS Bioscience Inc., and maintained in DMEM (GenDEPOT, LLC) plus 10% fetal calf serum (Gibco; Thermo Fischer Scientific, Inc.) and 1% penicillin/streptomycin. Human CRC cell lines HCT116, SNU283, HCT8 (colon; colorectal) and HT29, DLD-1 (colon) were purchased from Korea Cell Line Bank (Seoul, Korea) and analyzed by STR profiling. HCT116 p53 knockout cell line was provided from the Keck School of Medicine of USC (Professor LIN ZHANG). Cells were cultured in RPMI-1640 medium (GenDEPOT, LLC) with 10% fetal bovine serum (Gibco; Thermo Fischer Scientific, Inc.), 1 mM L-glutamine, 26 mM sodium bicarbonate and 1% P/S (penicillin/streptomycin). All cells were cultured at 37˚C in a 5% CO_2 incubator. All cell lines were confirmed not to be infected with mycoplasma using a mycoplasma detection kit (cat. no. SMD0173; BIOMAX).

Reagents and antibodies. The FDA-approved drug library (1,018 drugs), vismodegib and daunorubicin were purchased from Selleck Chemicals. BODIPY-cyclopamine was obtained from BioVision, Inc. Oxaliplatin and Irinotecan were purchased from Sigma-Aldrich; Merck KGaA. Z-VAD-FMK (Promega Corporation) was treated at 25 μM as a caspase inhibitor. Anti-SMO/Smoothened (1:1,000; cat. no. sc-166685;), anti-Lamin B (1:1,000; cat. no. sc-6216), Anti-Bcl-2 (1:1,000; cat. no. sc-509), anti-Bcl-xL (1:1,000; cat. no. sc-8392), anti-Bax (1:1,000; cat. no. sc-20067), anti-survivin (1:1,000; cat. no. sc-17779), anti-p53 (1:1,000; cat. no. sc-126), anti-p21 (1:1,000; cat. no. sc-397), anti-p300 (1:1,000; cat. no. sc-32244) and anti-PCAF (1:1,000; cat. no. sc-13124) antibodies were all purchased from Santa Cruz Biotechnology, Inc. Anti-PTCH/Patched (1:1,000; cat. no. 2468S), anti-β-tubulin (1:1,000; cat. no. 2126S), anti-Mcl-1 (1:1,000; cat. no. 4572S), anti-Bak (1:1,000; cat. no. 12105S), Anti-XIAP (1:1,000; cat. no. 2042S), anti-Bid (1:1,000; cat. no. 2002S), anti-Puma (1:1,000; cat. no. 4976S), anti-NOXA (1:1,000; cat. no. 14766S), Anti-BIM (1:1,000; cat. no. 2933S), anti-GLI1 (1:500; cat. no. 3538S), anti-GLI2 (1:1,000; cat. no. 2585S), anti-cleaved poly (ADP-ribose) polymerase (c-PARP) (1:1,000; cat. no. 9541S), anti-PARP (1:1,000; cat. no. 9542S), anti-c-caspase-3 (1:1,000; cat. no. 9664S), Anti-caspase-3 (1:1,000; cat. no. 9662S), anti-caspase-9 (1:1,000; cat. no. 9502S), anti-c-caspase-8 (1:1,000; cat. no. 9496S), anti-caspase-8 (1:1,000; cat. no. 4790T), anti-β-TrCP (1:1,000; cat. no. 4394S) and horseradish peroxidase (HRP)-conjugated anti-rabbit (1:2,000; cat. no. 7074S) were purchased from Cell Signaling Technology, Inc. Mouse IgG secondary antibodies

(1:2,000; cat. no. 170-6516) were purchased from Bio-Rad Laboratories, Inc. Anti-GLI3 (1:1,000; cat. no. A303-417) was purchased from Bethyl Laboratories, Inc. Anti-β-actin antibody (1:20,000; cat. no. A5316) was purchased from Sigma-Aldrich; Merck KGaA. Human phospho-kinase antibody array (cat no. ARY003B) was acquired from R&D Systems, Inc. Scrambled small interfering (si)RNA and AKT siRNA, ERK siRNA, PCAF siRNA and β-TrCP siRNA were purchased from Santa Cruz Biotechnology, Inc. Lipofectamine RNAi Max reagent (Thermo Fisher Scientific, Inc.) was used for siRNA transfection.

GLI-luciferase reporter gene assay. NIH3T3 cell lines stably expressing GLI-luciferase reporter construct were seeded at a rate of 25,000 cells/100 μl per well in 96-well tissue culture-treated plates. After overnight 37˚C incubation, 500 nl of pre-plated compounds dissolved in DMSO were pin-transferred to the cells using a Janus automated liquid handler workstation (PerkinElmer, Inc.) and incubated at 37˚C for 24 h. Bright-Glo luciferase assay reagent (Promega Corporation) was added to the cells according to the manufacturer's instructions, and the emitting luminescence (560 nm) was read using an Envision plate reader (PerkinElmer, Inc.).

Nuclear cytosol fractionation assay. The cytoplasmic and nuclear fractions were extracted using NE-PER™ Nuclear and Cytoplasmic Extraction Reagents (Thermo Fisher Scientific, Inc.). The harvested cells were washed with trypsin-EDTA, then centrifuged at 500 x g for 5 min at 4˚C. Cold CER I was added to the pellet, vortex followed, and then incubation on ice for 10 min. CER II was added, followed by brief vortex, and the pellet was centrifuged at 16,000 x g for 5 min at 4˚C to transfer the supernatant (cytoplasmic extract) to a new EP tube. NER was added in the tube with the pellet and placed it on ice for 40 min, with vortex performed every 10 min. After centrifugation at 16,000 x g for 10 min at 4˚C, the supernatant (nuclear extract) was then transferred to a new tube. Following quantification, western blot analysis was performed.

MTT cell viability assay. Cells (5,000 cells/100 μl per well) were seeded in 96-well tissue culture-treated plates. After one day, 500 nl of each pre-plated serially diluted daunorubicin (7 point, 5-fold serial dilution from 4 mM in DMSO) was pin-transferred to the assay plate. After 24 h, MTT reagents (Promega Corporation) were added as per the manufacturer's instructions and dissolved in 100 μl of DMSO after 4 h and the resulting absorption signals were read at 570 nM using Envision plate reader (PerkinElmer, Inc.). The GI_{50}s were calculated using Prism8 software (GraphPad Software Inc.; Dotmatics).

Western blotting. Cells were lysed with RIPA buffer containing 50 mM Tris-HCl pH 7.4, 150 mM NaCl, 0.1% SDS, 1% Triton X-100, and 1% sodium deoxycholate, protease and phosphatase inhibitor cocktail (Sigma-Aldrich; Merck KGaA). The BCA protein assay was used to measure protein concentration with a NanoDrop 2000c spectrophotometer (Software: NanoDrop 2000/2000c, version: 1.6.198, Thermo Fisher Scientific, Inc.) Thermo Fisher Scientific, Inc.) Equal amounts (50 μg) of proteins were loaded on 8, 10 and 12% SDS-PAGE according to size and then relocated to nitrocellulose membranes (Cytiva). At this point, the membranes were blocked with 5% skim milk with TBS containing 0.1% Tween 20 for 2 h at 4˚C. After blocking the membranes, they were incubated with the primary antibodies overnight at 4˚C. After being incubated overnight at 4˚C, they were incubated with HRP-labeled secondary antibodies for 2 h at 4˚C. ECL western blotting substrate (DoGenBio) was added, and the resulting signals were detected using X-ray films.

Transfection. Con siRNA (cat. no. sc-37007), GLI1 siRNA (cat. no. sc-37911), AKT siRNA (cat. no. sc-43609), ERK siRNA (cat. no. sc-29307, sc-35335), PCAF siRNA (cat. no. sc-36198) and β-TrCP siRNA (cat. no. sc-37178) were all purchased from Santa Cruz Biotechnology, Inc (The siRNA sequence is unavailable by Santa Cruz Biotechnology, Inc). HCT116 cells ($2x10^6$) were incubated with 200 nM siRNA using Lipofectamine RNA iMAX for 6 h at 37˚C. After 6 h, HCT116 cells were harvested after treatment with daunorubicin for 24 h.

Immunoprecipitation. Cells were lysed with 300 μl of lysis buffer (1 mM PMSF, protease inhibitors and phosphatase inhibitors) and analyzed for their content of bicinchoninic acid. A total of 50 μl protein G PLUS-Agarose beads were added to the supernatant for 1 h after the 2 μg primary antibodies (GLI1, ITCH, β-TrCP and PCAF) were incubated with it overnight at 4˚C. Immunoprecipitants were washed and isolated by centrifugation at 17,000 x g for 10 min and heated with a 2X sample buffer. Lastly, western blotting was used to analyze the supernatant.

Colony formation assay. A colony is defined to consist of at least 50 cells. HCT-116 cells were seeded at a density of $5x10^2$ cells/well in six-well plates and then incubated at 37˚C with a 5% CO_2 incubator. The medium was changed two to three times per week. After two weeks, cells were washed with DPBS (Dulbecco's phosphate buffered saline), fixed with 4% paraformaldehyde for 30 min, then stained with 0.5% crystal violet for 30 min at room temperature (RT) for visualization and cell counting.

Flow cytometric analysis of cell apoptosis. As an apoptosis marker, the translocation flipping of phosphatidylserine from the inner membrane to the outer leaflet of the plasma membrane was detected through the binding of fluorescein isothiocyanate (FITC)-conjugated annexin V. Briefly, HCT116 cells ($5x10^5$) were either untreated or treated with daunorubicin, then resuspended in the binding buffer of the Annexin V-PI Apoptosis Detection Kit (cat. no. 556547; BD Biosciences). Cells were then mixed with annexin V-FITC and propidium iodide (PI) before being incubated at 4˚C for 30 min in the dark. At this point, flow cytometry was immediately used to evaluate the cells (Navios EX flow cytometer; Beckman Coulter, Inc.).

Reverse transcription-quantitative PCR (RT-qPCR). Total RNAs were extracted using TRIzol reagent (Molecular Research Center, Inc.). The amplification of transcripts was executed using a reverse transcriptase PCR kit (Thermo Fisher Scientific, Inc.) in accordance with the manufacturer's

instructions. RT-qPCR was carried out on a Applied Biosystems® QuantStudio™ 6 Flex Real-Time PCR using gene-specific Taqman™ probes (Applied Biosystems; Thermo Fisher Scientific, Inc.). The 45 cycle PCR stage consisted of 2 steps: Denaturation step, 15 sec at 95˚C; combined annealing and extension step, 1 min at 60˚C. The Taqman™ probes were GAPDH (Hs99999905_m1), GLI1 (HS01110766_m1), Cyclin D1 (Hs00765553_m1), Snail (Hs00195591_m1), and Myc (Hs00153408_m1). (The sequence is unavailable by Thermo Fisher Scientific, Inc.) The mRNA expression was normalized to expression values of GAPDH. The relative gene expression ratios were analyzed using the $2^{-\Delta\Delta Cq}$ method (17).

Immunofluorescence staining. HCT-116 cells ($1x10^5$) were cultured on glass coverslips within a 12-well plate and fixed with 3.7% formaldehyde for 30 min at RT. With 0.5% Triton X-100, cells were permeable for 30 min at RT, then blocked using 1% bovine serum albumin (Thermo Fisher Scientific, Inc.) for 2 h. After blocking, HCT-116 cells were incubated with primary antibodies overnight at 4˚C. Next, the cells were washed for 30 min at RT and incubated with Alexa Fluor® 594-conjugated secondary antibody (1:200; cat. no. A-11005; Invitrogen; Thermo Fisher Scientific, Inc.). DAPI (1 μg/ml) was then used to counterstain the nuclei. Lastly, the cells were covered with VECTASHIELD mounting medium (Vector Laboratories, Inc.) and then visualized through fluorescence microscopy.

Caspase 3/7 activity measurement. Cells were plated in a 96-well white-wall plate at $8x10^3$ cells per well, in triplicate. After being treated with daunorubicin (0, 0.5 and 1 μM) for 24 h, 100 μl of Caspase-Glo 3/7 reagent (Promega Corporation) was added to each well. After 2 h of incubation in the dark, the caspase-3/7 activities were measured using a Varioskan Lux reader (Thermo Fisher Scientific, Inc.). Differences in caspase-3/7 activity between the drug-treated cells and untreated cells were expressed in terms of fold-change in luminescence.

MG132 and leupeptin treatment. HCT-116 cells were seeded at a density of $7x10^3$ cells/60 mm culture dish and then incubated at 37˚C in a 5% CO_2 incubator. The next day, cells were treated with 1 μM daunorubicin. After 18 h of treatment, cells were incubated with 2 μM MG132 (cat. no. 474790) or 100 rM Leupeptin (cat. no. L5793; both from Sigma-Aldrich; Merck KGaA) for 6 h. The cells were harvested after 6 h by centrifugation at 17,000 x g for 10 min at 4˚C.

Cycloheximide (CHX) assay. HCT-116 cells were seeded at a density of $7x10^3$ cells/60 mm culture dish and then incubated at 37˚C in a 5% CO_2 incubator. The next day, cells were pre-treated with 1 μM daunorubicin. And then, cells were harvested at 0, 1, 4 and 7 h after the following treatment with 200 μg/ml CHX (Sigma-Aldrich; Merck KGaA).

Tumor xenograft experiment. Animal experiments were implemented according to the animal care guidelines approved (approval no. KOREA-2020-0174) by the Korea University Institutional Animal Care and Use Committee (Seoul, Korea). Four-week-old female BALB/c nude mice (n=10; body weight, ±15 g) were purchased from Orient Bio, Inc. and contained in a specific pathogen-free environment. Prior to the experiment, the animals were housed for a week for acclimation and given free access to food and water. The temperature was maintained at 20-24˚C, with a relative humidity of 45-65% and a 12/12-h light/dark cycle. A total of 100 μl of HCT116 cells ($2x10^6$) in culture medium were implanted subcutaneously in the dorsal flank of 5-week-old BALB/c nude female mice. The tumor size was measured every two days. After the tumors reached a size of 100 mm^3, the nude mice were injected intraperitoneally with either vehicle (DMSO) or daunorubicin (2 mg/kg) every two days for 15 days. The experiment was terminated before the tumor size reached 1,000 mm^3, and the mice were sacrificed by inhaling 30% CO_2 (4.5 l/min) for 2 min in a CO_2 gas chamber. A total of 5 min later, after confirming that rigor mortis had occurred, the tumor tissue was removed.

Immunohistochemistry (IHC) staining. Sections (4-μm thickness) of formalin-fixed, paraffin-embedded tumor tissue were deparaffinized in xylene and hydrated in a graded alcohol series. To block endogenous peroxidase, 3% hydrogen peroxide was used for 15 min, and for antigen retrieval, heating at 100˚C for 20 min was used. A universal blocking solution was applied to the tissue slides for 15 min at RT, followed by an overnight incubation with primary antibodies at 4˚C. At RT, the samples were incubated with peroxidase-conjugated anti-goat IgG for 1 h. The EnVision Plus system (Dako; Agilent Technologies, Inc.) was used to visualize IHC responses using diaminobenzidine staining. Antibodies used in this method (including supplier, catalogue number and dilution) are listed in Table I. The staining intensity was divided into 5 grades, as shown in Table II.

TUNEL staining. Paraffin-embedded tumor tissues were deparaffinized in xylene and hydrated in a graded alcohol series (100% xylene for 3 min x 3, 100% ethanol for 1 min x 2, 95% ethanol for 1 min x 2, 70% ethanol for 1 min). Using the *in situ* cell death detection kit TMR red (cat. no. 12156792910; Roche Diagnostics) in accordance with the manufacturer's instructions, TUNEL staining was carried out. After TUNEL staining and mounting, a solution containing DAPI was applied (ProLongTM Gold antifade reagent with DAPI; cat. no. REFP36935; Invitrogen; Thermo Fisher Scientific, Inc.). Following mounting, the slides were examined using a fluorescence microscope (HC-010_LSM900/Super-Resolution laser Scanning Microscope) with excitation wavelengths of 488 and 640 nm. The observation process was performed at the top, middle, and bottom of each slide and the average value was recorded.

Combination index (CI) and statistical analysis. The CI method of Chou-Talalay (18,19) was used to analyze drug effects in order to determine whether the cytotoxic interactions of daunorubicin and irinotecan were synergistic, additive, or antagonistic in CRC cells. All statistics were analyzed using the GraphPad InStat 8 software (GraphPad Software Inc.; Dotmatics). One-way ANOVA was used for group comparisons, followed by Tukey's post hoc tests. Unpaired t-tests were used to determine significance between

Table I. Antibodies used for immunohistochemical staining.

Antibody	Supplier	Catalogue number	Dilution
GLI1	Novus Biologicals, LLC	NB600-600	1:400
p53	Santa Cruz Biotechnology, Inc.	SC-126	1:600

Table II. Immunohistochemical scoring.

Percentage score	Observation	Intensity score	Observation
1	0-5%	0	None
2	6-25%	1	White brown
3	26-50%	2	Brown
4	51-75%	3	Dark brown
5	76-100%		

two groups. $P<0.05$ was considered to indicate a statistically significant difference.

Results

Daunorubicin inhibits GLI1 activity in CRC cells. In an attempt to identify a new antagonist of the Hh pathway, an FDA-approved drug library comprised of 1,018 drugs was screened against the commercially available NIH3T3 cell line that stably expresses the GLI-dependent firefly luciferase reporter. As a result, it was found that 10 drugs inhibited GLI luciferase activity (Fig. S1A). As shown in Fig. S1B, among the 10 drugs examined, only daunorubicin and pralatrexate were demonstrated to decrease GLI1 in HCT116, a CRC cell. It was discovered that daunorubicin suppresses the activity of GLI-driven luciferase (Fig. 1A and B). Next, HCT116 cells were treated with daunorubicin (0, 0.5 and 1 μM) for 24 h and the protein levels of the components involved in the canonical Hh pathway were examined. None of SHH, GLI2, GLI3, Smo and Ptch1 protein levels were significantly changed by daunorubicin (Figs. 1C-E and S2A). Moreover, daunorubicin was shown to downregulate GLI1 protein levels in other CRC cells, including HT29 and SNU283 cells (Fig. S2B). The mRNA expression level of GLI1, cyclin D1, Snail and Myc was significantly downregulated (Fig. 1D). Western blot analysis of the cytoplasmic and nuclear extractions of HCT116 cells revealed that daunorubicin treatment downregulated nuclear expression of GLI1 when compared with the control (Figs. 1F and S2C). These results indicated that daunorubicin inhibits GLI1 expression.

Daunorubicin induces caspase-dependent apoptosis in HCT116 cells. First, to examine the cytotoxicity of daunorubicin in CRC cells (Fig. 2A), various CRC cell lines were cultured with different concentrations (0-20 μM) of daunorubicin for 24 h. The survival of CRC cell lines HCT116, HT29 and SNU283 with high expression of GLI1 was reduced by daunorubicin in a dose-dependent manner. On the other hand, DLD-1 and HCT8 with low GLI1 expression showed less reduction by daunorubicin. Furthermore, to confirm the daunorubicin reduced cell proliferation in CRC cells, a colony forming assay was performed in HCT116 cells. As demonstrated in Fig. 2B, colony formation was strongly inhibited in HCT116 cells. Moreover, to examine whether the cell death induced by the treatment promoted apoptosis, Annexin V-PI staining was conducted along with the treatment of daunorubicin at 0, 0.5 and 1 μM for 24 h of HCT116 cells in a dose-dependent manner in a flow cytometric analysis (Fig. 2C). Caspase-3/7 activity was also augmented in a dose-dependent manner (Fig. 2D). Daunorubicin increased the levels of c-PARP, caspase-8, caspase-9 and caspase-3, which were suppressed by co-treatment of a pan-caspase inhibitor z-VAD-fmk, thus indicating that daunorubicin induced caspase-dependent apoptosis in HCT116 cells (Figs. 2E and S3A). To determine whether cell death is affected by the expression of GLI1, GLI1 was knocked down in the HCT116 cells. As revealed in Fig. 2F and G, when GLI1 was knocked down, daunorubicin-induced cell death and c-PARP, caspase-8, caspase-9 and caspase-3 were not increased (Figs. 2F, 2G and S3B). Therefore, the aforementioned results suggested that the daunorubicin induces caspase-dependent apoptosis through inhibition of GLI1 in CRC.

Daunorubicin induces p53-mediated apoptosis and GLI1 downregulation in HCT-116 cells. To determine whether GLI1 inhibition by daunorubicin occurs by the canonical or non-canonical pathway, it was attempted to demonstrate this by inhibiting AKT or ERK, which are representative non-canonical Hh signaling pathways. When inhibiting AKT or ERK, decreased cell survival and inhibition of GLI1 expression by daunorubicin was observed (Figs. 3A, S4A and B). These results indicated that inhibition of GLI1 by daunorubicin occurs through the canonical Hh pathway.

A human phospho-kinase antibody array was then used to investigate which pathways are regulated by daunorubicin (1 μM). Interestingly, among the phosphorylation on the protein array, the p53 phosphorylation (S15, S46 and S392) was shown to be markedly increased by daunorubicin treatment (Fig. 3B). These results indicated the existence of daunorubicin-induced p53 activation. Furthermore, daunorubicin also enhanced the phosphorylation of Chk2 (T68) (20) and p27 (T198) (21), both of which are involved in cell cycle arrest (Fig. 3B). The levels of apoptosis-related marker proteins were also examined. Consistent with the results provided in Fig. 3B, daunorubicin increased the levels of pro-apoptotic proteins such as p53, Bim, Bak, Bax and c-PARP, while it decreased the levels of anti-apoptotic Cyclin D1 (Figs. 3C and S5A). In the HCT116 p53 knockout cell line, daunorubicin-induced PARP cleavage and p21 did not increase, while the decreased

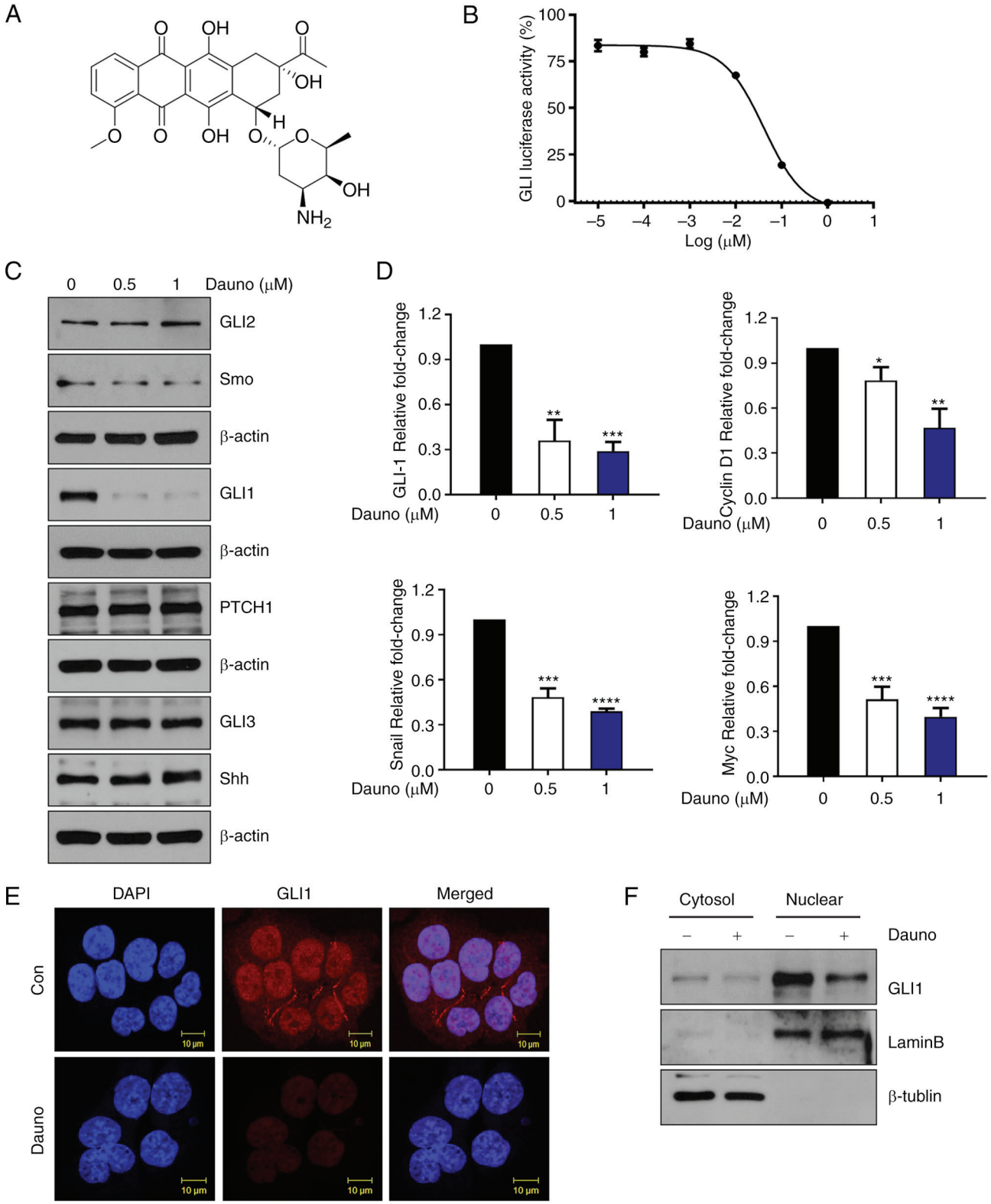

Figure 1. Daunorubicin suppresses Hh signaling in HCT-116 cells. (A) Daunorubicin structure. (B) Titration of daunorubicin against GLI-dependent luciferase reporter assay. (C and D) Daunorubicin-induced GLI1 downregulation of protein and mRNA levels of the main components involved in the Hh pathway after treatment with daunorubicin (0.5 and 1 μM) for 24 h. (E and F) GLI1 expression of cytosol and nucleus in (E) immunostaining and (F) western blot analysis. β-tubulin and lamin B were used as a marker for each fraction. Scale bar, 10 μm. The data are expressed as the mean of 3 independent experiments. *P<0.05, **P<0.005, ***P<0.001 and ****P<0.0001. Hh, Hedgehog.

expression of GLI1 and CyclinD1 was significantly reversed compared with the HCT116 wild-type cells. This suggested that daunorubicin induces apoptosis through p53 activation (Figs. 3D and S5B). The activation of p300 and PCAF is necessary for the p53-dependent response to genotoxic stress, according to a common mechanism (22). As previously

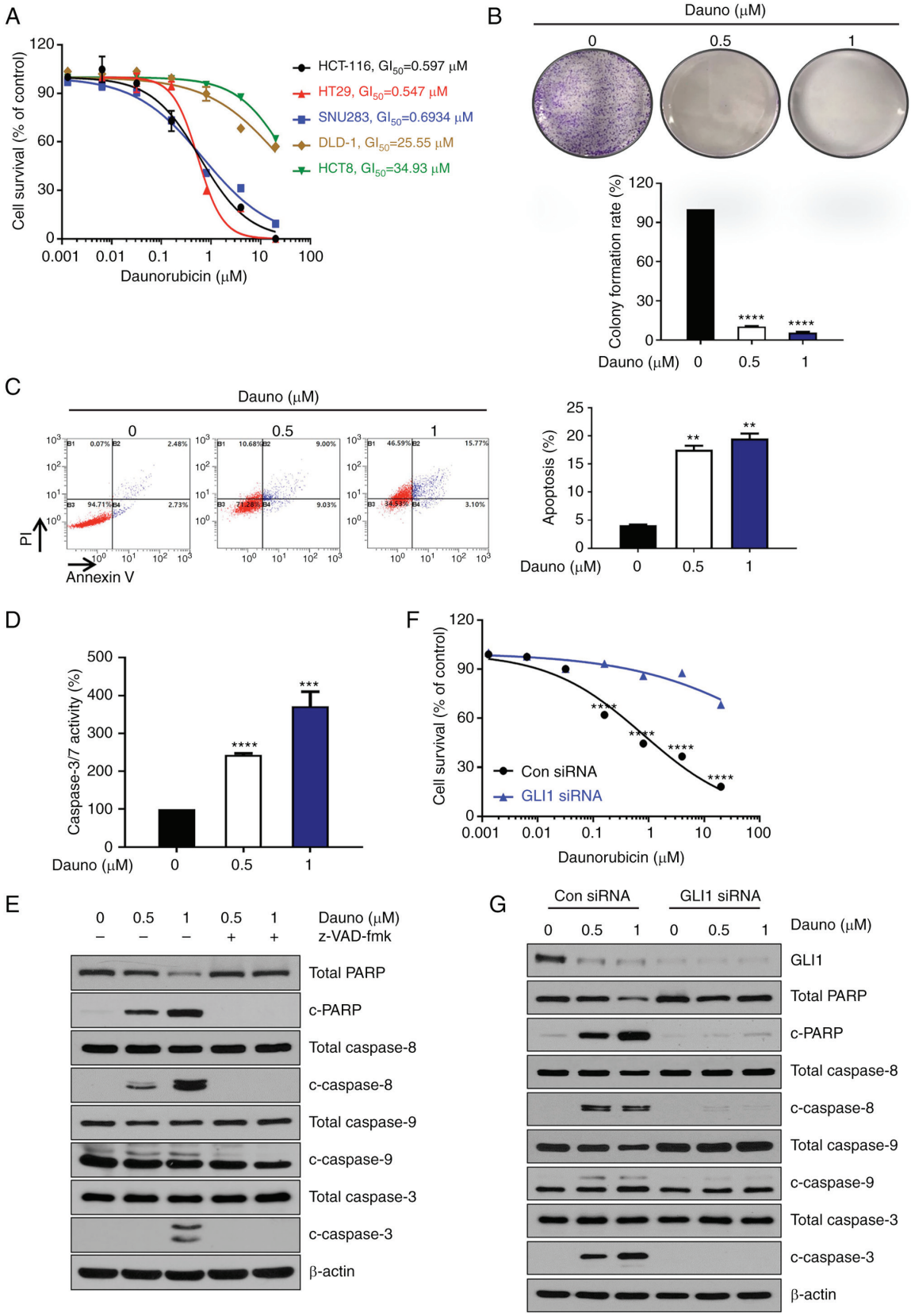

Figure 2. Daunorubicin-induced caspase-dependent apoptosis in HCT116 cells. (A) Daunorubicin decreased the proliferation of HCT116, HT29, SNU283, DLD-1 and HCT8 cells with GI_{50} of 0.597, 0.547, 0.6934, 25.55 and 34.93 μM, respectively. (B) Colony formation assay using HCT116 cells after treatment of daunorubicin (0, 0.5 and 1) and quantitation. (C) Treatment of daunorubicin (0, 0.5 and 1 μM) for 24 h-induced apoptosis of HCT116 cells in a dose-dependent manner. Quantitation of cell death is plotted on the right. The graph was drawn by combining the B2 and B4 quadrants. (D) Treatment of daunorubicin (0, 0.5 and 1 μM) for 24 h led to a dose-dependent increase in caspase3/7 activity. (E) HCT116 cells were pretreated with 25 μM z-VAD-fmk for 30 min and then treated with daunorubicin (0, 0.5 and 1 μM). Western blotting was used to measure the expression levels of c-PARP, caspase3, caspase9 and caspase8. (F) After GLI1 knockdown using GLI1 siRNA, cell survival induced by daunorubicin was detected. (G) After GLI1 knockdown using GLI1 siRNA, western blotting was used to measure the expression levels of c-PARP, caspase3, caspase9 and caspase8. The data are expressed as the mean of 3 independent experiments. **P<0.005, ***P<0.001 and ****P<0.0001. siRNA, small interfering RNA; c-PARP, cleaved poly (ADP-ribose) polymerase.

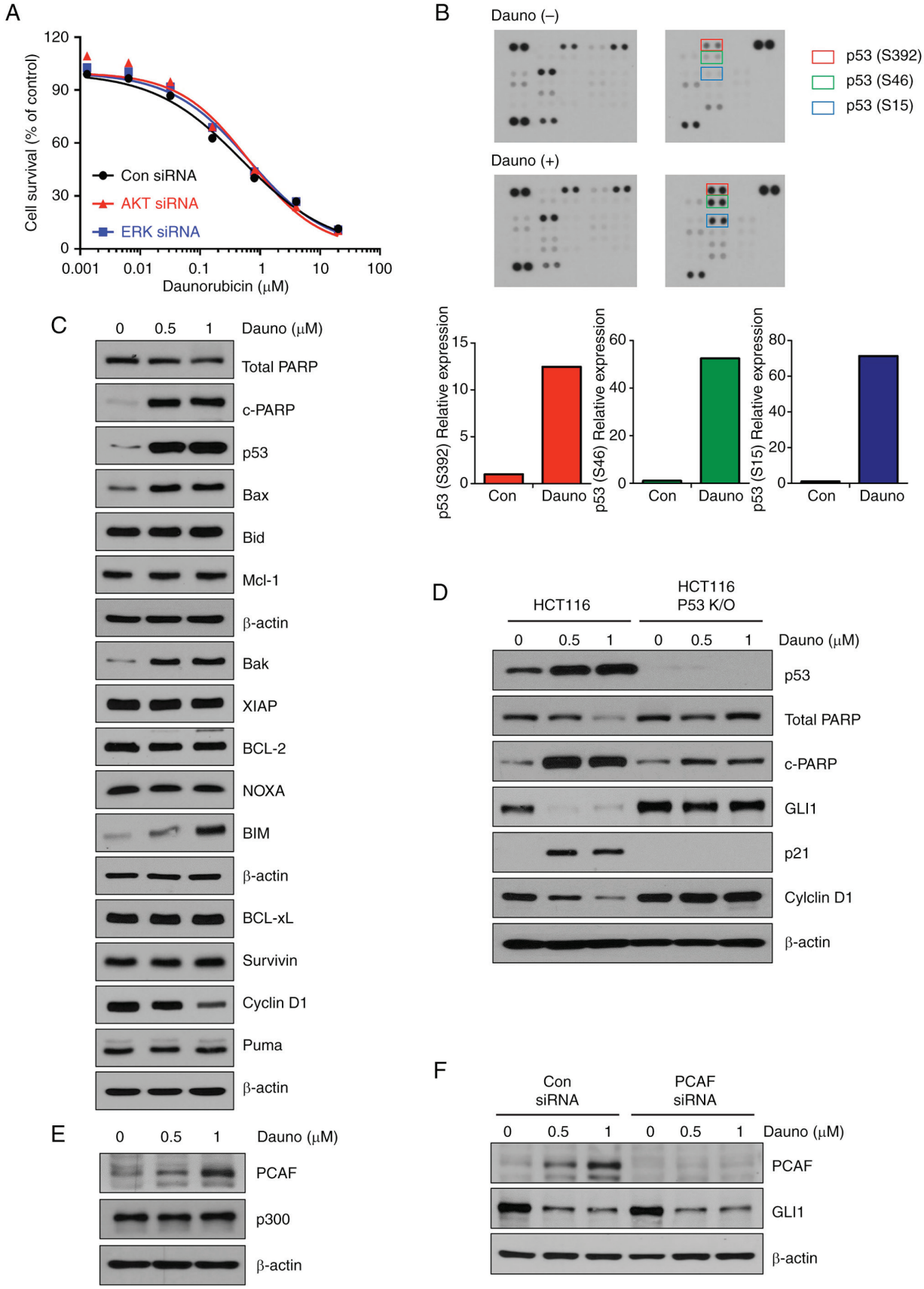

Figure 3. Daunorubicin induces p53-mediated apoptosis and GLI1 downregulation in HCT116 cells. (A) After AKT or ERK knockdown using siRNA, cell survival induced by daunorubicin was detected. (B) A phospho-kinase antibody array analysis showed that daunorubicin substantially increased p53 phosphorylation (S15, S46 and S392). The quantitation is depicted in the lower panel. (C) Western blot analysis for apoptosis-related marker proteins following treatment of daunorubicin (0.5 and 1 μM) for 24 h. (D) Western blotting was used to measure the expression levels of c-PARP, p53, GLI1, p21 and Cyclin D1 in HCT116 and HCT116 p53 knockout cells. (E) Western blot analysis for PCAF and p300 following treatment of daunorubicin (0.5 and 1 μM) for 24 h. (F) Results of daunorubicin (0.5 and 1 μM) treatment for 24 h after PCAF knockdown using PCAF siRNA. The data are expressed as the mean of 3 independent experiments. siRNA, small interfering RNA; K/O, knockout; c-PARP, cleaved poly (ADP-ribose) polymerase.

reported, it has been demonstrated that upregulation of PCAF induced by p53 is required for the suppression of GLI1 in response to DNA damage (23). It was investigated whether the expression levels of PCAF and P300 were changed by daunorubicin. Daunorubicin increased the expression of PCAF in a dose-dependent manner (Figs. 3E and S5C). To confirm whether the PCAF-dependent suppression of GLI1 occurred, PCAF was knocked down using PCAF siRNA. By demonstrating that GLI1 was still reduced by daunorubicin despite PCAF suppression, these results proved that the inhibition of GLI1 by daunorubicin was not dependent on PCAF (Figs. 3F and S5D).

Daunorubicin promotes GLI1 ubiquitination and proteasomal degradation. Daunorubicin did not displace the BODIPY-cyclopamine from Smo in HCT116 cells, indicating that daunorubicin does not bind to Smo (Fig. S6); therefore, it was investigated how it regulates the downstream GLI1. Treatment with MG132, a proteasome inhibitor, and leupeptin, a lysosome inhibitor, was administered to investigate whether the reduction of GLI1 was attributable to proteasomal or lysosomal degradation. The GLI1 expression decreased by daunorubicin was increased by MG132 and not changed by leupeptin (Figs. 4A and S7A). These data demonstrated that the reduction of GLI1 by daunorubicin was caused by proteasome degradation. Moreover, HCT116 cells were treated with CHX, a protein synthesis inhibitor. The expression of GLI1 was significantly reduced when HCT116 cells were exposed to daunorubicin and CHX compared with when they were exposed to CHX alone, thus suggesting that daunorubicin decreased the level of GLI1 through ubiquitin-proteasome degradation (Fig. 4B). These results confirmed that daunorubicin promotes the ubiquitination of GLI1 (Figs. 4C and S7B). To investigate what E3 ligase is responsible for the GLI1 ubiquitination, immunoprecipitation was performed to measure the interaction between GLI1 and E3 ligase. As shown in Fig. 4D, daunorubicin increased interaction between GLI1 and β-TrCP (Figs. 4D and S7C). To investigate whether β-TrCP-dependent GLI1 ubiquitination occurred, β-TrCP was knocked down using β-TrCP siRNA. Knockdown of β-TrCP restored the daunorubicin-induced reduction of GLI1, and the ubiquitination of GLI1 was also unchanged (Figs. 4E and S7D). These data suggested that daunorubicin induces GLI1 ubiquitination via β-TrCP.

Daunorubicin inhibits Hh pathway and induces apoptosis in HCT116 xenograft in vivo mouse model. HCT116 cells ($2x10^6$) were subcutaneously injected into BALB/c nude mice. When the size of the tumors was 100 mm^3, nude mice were treated with daunorubicin (2 mg/kg) every two days for 15 days by intraperitoneal injection. The tumor growth and weight were repressed in the daunorubicin-treated group compared with the control group (Fig. 5A-C), while body weight did not significantly differ between the control and daunorubicin-treated groups (Fig. 5D). These data indicated that daunorubicin induced apoptosis. Consistent with the *in vitro* results, IHC showed significant suppression of GLI1 levels in the daunorubicin-treated group in addition to increased p53 (Fig. 5E). A TUNEL assay indicated daunorubicin-induced apoptosis in tumor tissues (Fig. 5F). Taken together, these results indicated that daunorubicin exhibited anticancer effects in the CRC xenograft mice, in part through GLI1 downregulation.

In addition, it was confirmed whether daunorubicin had a combined effect with oxaliplatin or irinotecan, which are representative anticancer drugs used for CRC. As demonstrated in Fig. S8, a combined effect of daunorubicin and irinotecan was observed. Additional research is needed to confirm the possibility of future combinatory use.

Discussion

Daunorubicin is used as the first-line treatment for leukemia, and it is typically administrated in combination with other chemotherapeutic agents such as cytarabine (24). It has also been reported to have anticancer effects in monotherapy or combination therapy in solid tumors. It is well-established that the ability of daunorubicin to intercalate DNA and interfere with DNA replication process is the main mode of action for its anticancer effect. The results of the present study demonstrated that daunorubicin exerts anticancer activity in CRC in part through its ability to suppress the non-canonical Hh pathway.

From the screening using FDA-approved drug library, daunorubicin was identified as an inhibitor of Hh signaling. The results of the present study revealed that daunorubicin suppressed the Shh/Smo-independent non-canonical Hh pathway in CRC cells. It was found that daunorubicin suppresses GLI1 through (i) upregulating p53 and (ii) promoting β-TrCP-mediated GLI1 ubiquitination and the subsequent proteasomal degradation, which suppresses GLI1 function. It has been previously reported that p53 negatively regulates GLI1 function. A previous study revealed that p53 elevates the PCAF level, which consequently increases GLI1 ubiquitination and proteasomal degradation (23). However, in the present study, as demonstrated in Figs. 3 and 4, it was identified for the first time that daunorubicin suppresses GLI1 through B-TrCP, not through PCAF-induced reduction of GLI1.

In the present experimental condition, daunorubicin was not found to downregulate the protein levels of Ptch1 or Smo. Daunorubicin did not displace the BODIPY-cyclopamine from Smo in cells, implying that daunorubicin does not bind to Smo (Fig. S6). These results suggested that daunorubicin does not target Smo but inhibits Hh signaling through GLI1. Previous studies using patient samples revealed that the nuclear Smo is found in nearly 50% of patients with pancreatic cancer and CRC (25,26). Moreover, Rahman *et al* (27) identified that nuclear Smo acts as a Smo-independent Hh activation mechanism and confers resistance to Smo inhibitors. The present study demonstrated that daunorubicin strongly suppresses Hh signaling while also enhancing Smo in the nucleus. The daunorubicin-induced suppression of the non-canonical Hh pathway might overwhelm the Hh pathway activation exerted by the nuclear Smo. However, further research is needed to inspect whether the nuclear Smo induced by daunorubicin is functionally identical to the oncogenic nuclear Smo in cancer cells (27,28). In an *in vivo* study using a mouse xenograft of HCT116 cells, administration of daunorubicin (2 mg/kg, ip) was found to greatly

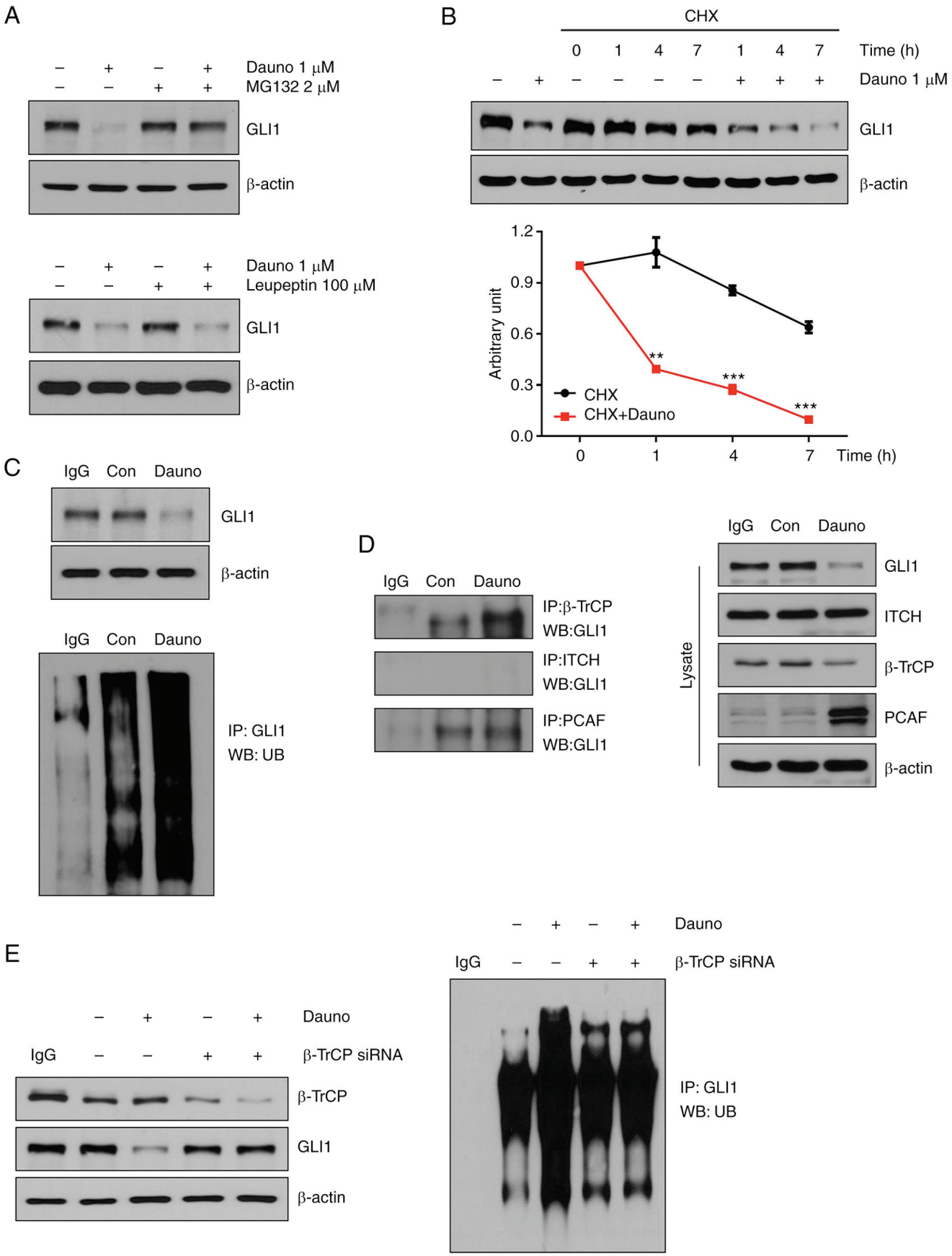

Figure 4. Daunorubicin promotes GLI1 ubiquitination and proteasomal degradation. (A) HCT116 cells were treated with 2 μM MG132 or 100 μM leupeptin. (B) CHX chase assay showed that daunorubicin reduced the stability of GLI1 protein. Quantitation of GLI1 is also plotted. (C and D) Daunorubicin promoted the ubiquitination of GLI1 in HCT-116 cells. Immunoprecipitation using antibodies against each of the three E3 ligases revealed a major enhancement of β-TrCP-GLI1 interaction. (E) Results of daunorubicin (1 μM) treatment for 24 h after β-TrCP knockdown using β-TrCP siRNA. Immunoprecipitation using GLI1 and β-TrCP antibody. The data are expressed as the mean of 3 independent experiments. **P<0.005 and ***P<0.001. CHX, cycloheximide; siRNA, small interfering RNA.

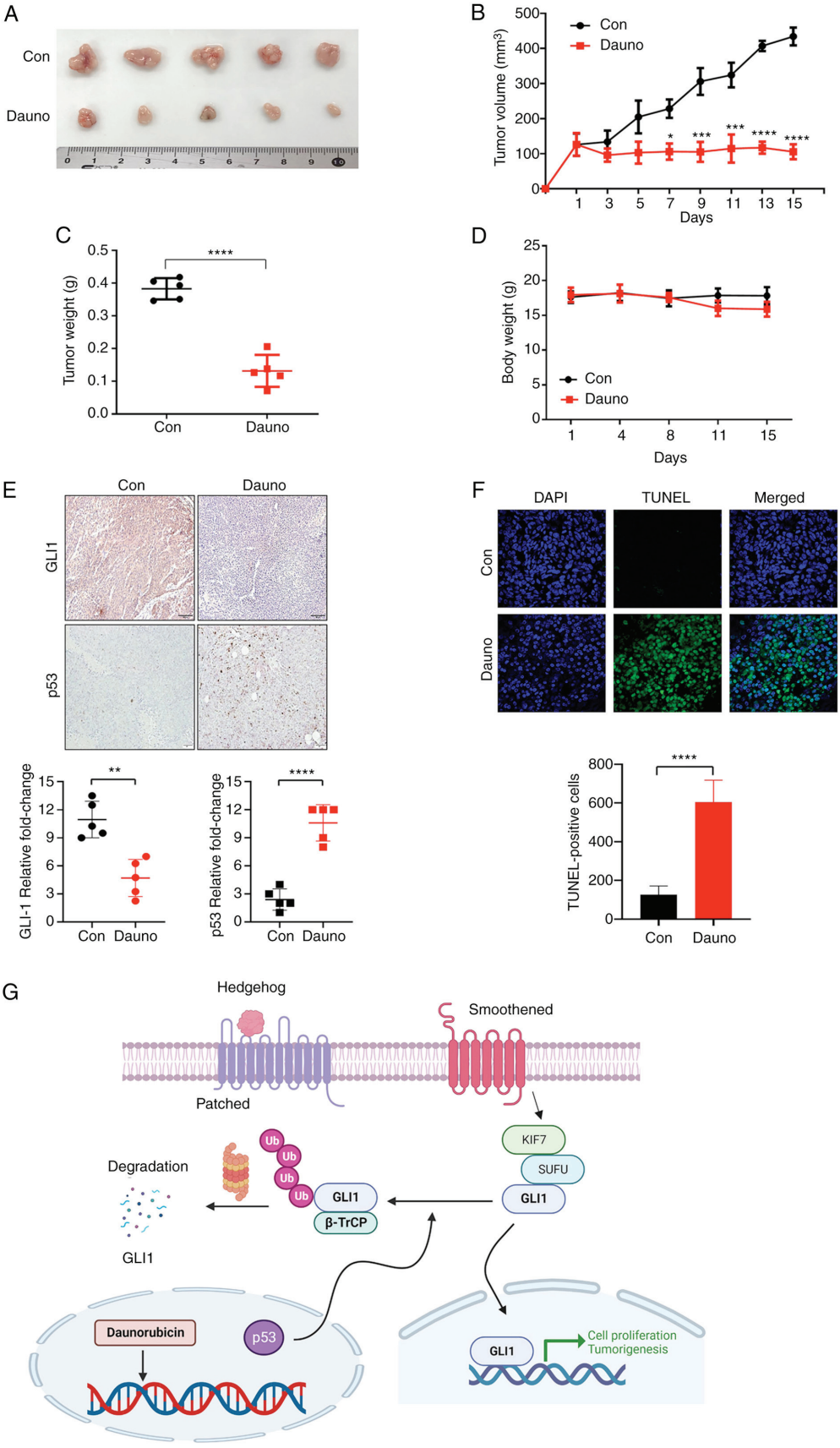

Figure 5. Daunorubicin inhibits the Hedgehog pathway and induces apoptosis in HCT116 xenograft *in vivo* mouse model. HCT116 cells ($2x10^6$) were subcutaneously injected into BALB/c nude mice. When the size of the tumors was 100 mm^3, the nude mice were randomized and treated with vehicle or daunorubicin (n=5, 2 mg/kg, ip, qod, 15 days). (A) Tumors in the daunorubicin-treated group and the control group after 15 days of treatment. (B) Average tumor volume plotted over the treatment period. (C) Tumor weights of daunorubicin-treated group and control group after 15 days of treatment. (D) Body weight change in drug-treated group and control group over the treatment period. (E) Immunohistochemistry of the tumor tissues using anti-GLI1 and p53 antibody after 15 days of treatment. (F) TUNEL assay after drug treatment for 15 days showed daunorubicin-induced apoptosis in tumor tissues. 20X. (G) Schematic representation of daunorubicin-induced apoptosis through the inhibition of GLI1 (created with BioRender.com). *P<0.05, **P<0.005, ***P<0.001 and ****P<0.0001.

suppress the tumor progress and GLI1 level in tumor tissues (Fig. 5).

Daunorubicin has been shown to have no effect in patients with advanced colorectal carcinoma in clinical trial II (29). However, the procedure was performed without selecting a patient group, and it is considered that daunorubicin would be effective in a patient group in which GLI1 was overexpressed.

Collectively, the present results revealed that daunorubicin suppresses Hh pathway in CRC. To the best of the authors' knowledge, this is the first study on the anticancer mechanism of daunorubicin with regard to the Hh pathway. The current study disclosed a new mode of daunorubicin's anticancer effect, and it may provide a rationale for expanding the clinical applicability of daunorubicin.

Acknowledgements

Not applicable.

Funding

The present was supported by the Basic Science Research Program through the National Research Foundation of Korea (NRF) funded by the Ministry of Education (grant no. RS-2023-00238158), the National Research Foundation of Korea (NRF) grant funded by the Korea government (MSIT) (grant no. NRF-2018M3A9G1075 561) and the Korea Institute of Science and Technology (grant no. 2E33131).

Availability of data and materials

The data generated in the present study may be requested from the corresponding author.

Authors' contributions

BRK, DYK and NLT performed most of the experiments and wrote the manuscript. BGK provided technical assistance. SIL, BYM and SHK contributed to conceptualization of the study and interpretation of results. SCO and WYH supervised the projects, provided funding and helped writing the manuscript. All authors read and approved the final manuscript. BRK and SCO confirm the authenticity of all the raw data.

Ethics approval and consent to participate

Animal experiments were implemented according to the animal care guidelines approved (approval no. KOREA-2020-0174) by the Korea University (Seoul, Korea) Institutional Animal Care and Use Committee (IACUC).

Patient consent for publication

Not applicable.

Competing interests

The authors declare that they have no competing interests.

References

1. Girardi D, Barrichello A, Fernandes G and Pereira A: Targeting the hedgehog pathway in cancer: Current evidence and future perspectives. Cells 8: 153, 2019.
2. Niyaz M, Khan MS and Mudassar S: Hedgehog signaling: An achilles' heel in cancer. Transl Oncol 12: 1334-1344, 2019.
3. Pak E and Segal RA: Hedgehog signal transduction: Key players, oncogenic drivers, and cancer therapy. Dev Cell 38: 333-344, 2016.
4. Sari IN, Phi LTH, Jun N, Wijaya YT, Lee S and Kwon HY: Hedgehog signaling in cancer: A prospective therapeutic target for eradicating cancer stem cells. Cells 7: 208, 2018.
5. Peer E, Tesanovic S and Aberger F: Next-generation hedgehog/GLI pathway inhibitors for cancer therapy. Cancers (Basel) 11: 538, 2019.
6. Katoh Y and Katoh M: Hedgehog target genes: Mechanisms of carcinogenesis induced by aberrant hedgehog signaling activation. Curr Mol Med 9: 873-886, 2009.
7. Barnes EA, Heidtman KJ and Donoghue DJ: Constitutive activation of the shh-ptc1 pathway by a patched1 mutation identified in BCC. Oncogene 24: 902-915, 2005.
8. Tao Y, Mao J, Zhang Q and Li L: Overexpression of hedgehog signaling molecules and its involvement in triple-negative breast cancer. Oncol Lett 2: 995-1001, 2011.
9. van den Brink GR, Bleuming SA, Hardwick JC, Schepman BL, Offerhaus GJ, Keller JJ, Nielsen C, Gaffield W, van Deventer SJ, Roberts DJ and Peppelenbosch MP: Indian hedgehog is an antagonist of Wnt signaling in colonic epithelial cell differentiation. Nat Genet 36: 277-282, 2004.
10. Yoshikawa K, Shimada M, Miyamoto H, Higashijima J, Miyatani T, Nishioka M, Kurita N, Iwata T and Uehara H: Sonic hedgehog relates to colorectal carcinogenesis. J Gastroenterol 44: 1113-1117, 2009.
11. Rajurkar M, De Jesus-Monge WE, Driscoll DR, Appleman VA, Huang H, Cotton JL, Klimstra DS, Zhu LJ, Simin K, Xu L, *et al*: The activity of Gli transcription factors is essential for Kras-induced pancreatic tumorigenesis. Proc Natl Acad Sci USA 109: E1038-E1047, 2012.
12. Wang Y, Ding Q, Yen CJ, Xia W, Izzo JG, Lang JY, Li CW, Hsu JL, Miller SA, Wang X, *et al*: The crosstalk of mTOR/S6K1 and hedgehog pathways. Cancer Cell 21: 374-387, 2012.
13. Pandolfi S, Montagnani V, Penachioni JY, Vinci MC, Olivito B, Borgognoni L and Stecca B: WIP1 phosphatase modulates the Hedgehog signaling by enhancing GLI1 function. Oncogene 32: 4737-4747, 2013.
14. Lauth M, Bergström A, Shimokawa T and Toftgard R: Inhibition of GLI-mediated transcription and tumor cell growth by small-molecule antagonists. Proc Natl Acad Sci USA 104: 8455-8460, 2007.
15. Agyeman A, Jha BK, Mazumdar T and Houghton JA: Mode and specificity of binding of the small molecule GANT61 to GLI determines inhibition of GLI-DNA binding. Oncotarget 5: 4492-4503, 2014.
16. Hyman JM, Firestone AJ, Heine VM, Zhao Y, Ocasio CA, Han K, Sun M, Rack PG, Sinha S, Wu JJ, *et al*: Small-molecule inhibitors reveal multiple strategies for Hedgehog pathway blockade. Proc Natl Acad Sci USA 106: 14132-14137, 2009.
17. Livak KJ and Schmittgen TD: Analysis of relative gene expression data using real-time quantitative PCR and the 2(-Delta Delta C(T)) Method. Methods 25: 402-408, 2001.
18. Chou TC: Theoretical basis, experimental design, and computerized simulation of synergism and antagonism in drug combination studies. Pharmacol Rev 58: 621-681, 2006.
19. Chou TC and Talalay P: Quantitative analysis of dose-effect relationships: The combined effects of multiple drugs or enzyme inhibitors. Adv Enzyme Regul 22: 27-55, 1984.
20. Garcia-Santisteban I, Llopis A, Krenning L, Vallejo-Rodríguez J, van den Broek B, Zubiaga AM and Medema RH: Sustained CHK2 activity, but not ATM activity, is critical to maintain a G1 arrest after DNA damage in untransformed cells. BMC Biol 19: 35, 2021.
21. De Vita F, Riccardi M, Malanga D, Scrima M, De Marco C and Viglietto G: PKC-dependent phosphorylation of p27 at T198 contributes to p27 stabilization and cell cycle arrest. Cell Cycle 11: 1583-1592, 2012.
22. Sakaguchi K, Herrera JE, Saito S, Miki T, Bustin M, Vassilev A, Anderson CW and Appella E: DNA damage activates p53 through a phosphorylation-acetylation cascade. Genes Dev 12: 2831-2841, 1998.

23. Mazzà D, Infante P, Colicchia V, Greco A, Alfonsi R, Siler M, Antonucci L, Po A, De Smaele E, Ferretti E, *et al*: PCAF ubiquitin ligase activity inhibits Hedgehog/Gli1 signaling in p53-dependent response to genotoxic stress. Cell Death Differ 20: 1688-1697, 2013.
24. Murphy T and Yee KWL: Cytarabine and daunorubicin for the treatment of acute myeloid leukemia. Expert Opin Pharmacother 18: 1765-1780, 2017.
25. Li T, Liao X, Lochhead P, Morikawa T, Yamauchi M, Nishihara R, Inamura K, Kim SA, Mima K, Sukawa Y, *et al*: SMO expression in colorectal cancer: Associations with clinical, pathological, and molecular features. Ann Surg Oncol 21: 4164-4173, 2014.
26. Maréchal R, Bachet JB, Calomme A, Demetter P, Delpero JR, Svrcek M, Cros J, Bardier-Dupas A, Puleo F, Monges G, *et al*: Sonic hedgehog and Gli1 expression predict outcome in resected pancreatic adenocarcinoma. Clin Cancer Res 21: 1215-1224, 2015.
27. Rahman MM, Hazan A, Selway JL, Herath DS, Harwood CA, Pirzado MS, Atkar R, Kelsell DP, Linton KJ, Philpott MP and Neill GW: A novel mechanism for activation of GLI1 by nuclear SMO that escapes anti-SMO inhibitors. Cancer Res 78: 2577-2588, 2018.
28. Niyaz M, Khan MS, Wani RA, Shah OJ, Besina S and Mudassar S: Nuclear localization and overexpression of smoothened in pancreatic and colorectal cancers. J Cell Biochem 120: 11941-11948, 2019.
29. Harvey J, Bonnem E, Grady K, Goodman A and Schein P: Phase II study of daunorubicin in previously untreated patients with advanced colorectal carcinoma. Med Pediatr Oncol 13: 30-31, 1985.

Copyright © 2024 Kim et al. This work is licensed under a Creative Commons Attribution-NonCommercial-NoDerivatives 4.0 International (CC BY-NC-ND 4.0) License.